Radiation Dosimetry and Biodistribution of the TSPO Ligand ^{11}C-DPA-713 in Humans

Christopher J. Endres[1], Jennifer M. Coughlin[2], Kenneth L. Gage[1], Crystal C. Watkins[2], Michael Kassiou[3–5], and Martin G. Pomper[1,2]

[1]Department of Radiology, Johns Hopkins Medical Institutions, Baltimore, Maryland; [2]Department of Psychiatry, Johns Hopkins Medical Institutions, Baltimore, Maryland; [3]Brain and Mind Research Institute, University of Sydney, New South Wales, Australia; [4]School of Chemistry, University of Sydney, New South Wales, Australia; and [5]Discipline of Medical Radiation Sciences, University of Sydney, New South Wales, Australia

Whole-body PET/CT was used to characterize the radiation dosimetry of ^{11}C-DPA-713, a specific PET ligand for the assessment of translocator protein. **Methods:** Six healthy control subjects, 3 men and 3 women, underwent whole-body dynamic PET scans after bolus injection of ^{11}C-DPA-713. Subjects were scanned from head to mid thigh with 7 passes performed, with a total PET acquisition of approximately 100 min. Time–activity curves were generated in organs with visible tracer uptake, and tissue residence times were calculated. Whole-body dosimetry was calculated using OLINDA 1.1 software, assuming no voiding. **Results:** The absorbed dose is highest in the lungs, spleen, kidney, and pancreas. The lungs were determined to be the dose-limiting organ, with an average absorbed dose of 2.01×10^{-2} mSv/MBq (7.43×10^{-2} rem/mCi). On the basis of exposure limits outlined in the U.S. Food and Drug Administration Code of Federal Regulations (21CFR361.1), the single-dose limit for ^{11}C-DPA-713 radiotracer injection is 2,487.6 MBq (67.3 mCi). **Conclusion:** ^{11}C-DPA-713 has an uptake pattern that is consistent with the biodistribution of translocator protein and yields a dose burden that is comparable to that of other ^{11}C-labeled PET tracers.

Key Words: radiotracer tissue kinetics; dosimetry; microglia; PET/CT; translocator protein

Translocator protein (TSPO), known formerly as the peripheral benzodiazepine receptor (PBR) (1), is established as an important marker of neuroinflammation in central nervous system disease or brain injury, as reviewed by various authors (2–5). Historically, the TSPO ligand used most commonly with PET is ^{11}C-R-PK11195. Although it has been used successfully for numerous clinical studies, ^{11}C-R-PK11195 has

pharmacokinetic properties, such as high nonspecific binding, that are suboptimal for imaging. Given the importance of TSPO as a molecular target, in recent years there has been tremendous interest in developing an alternative radiotracer for PET (6–9). One such ligand is ^{11}C-DPA-713 (10), which has been shown to have greater uptake and higher affinity than ^{11}C-R-PK11195 (11). However, it has also been shown that ^{11}C-DPA-713 is susceptible to multiple-affinity state binding (12,13). Nevertheless, ^{11}C-DPA-713 shows promise as a prospective TSPO ligand; thus, we evaluated the radiation dose burden in healthy human control subjects after bolus tracer injection.

MATERIALS AND METHODS

Human Subjects

Six healthy volunteers (3 women, 3 men) were included in this study (Table 1). Subjects with a history of recent nosocomial infection, central nervous system lymphoma, neurologic disorder, structural central nervous system abnormality, head injury, or active substance abuse were excluded from participating. Female subjects were also screened and excluded for pregnancy. This study was approved by the Johns Hopkins Institutional Review Board. Subjects received an explanation of the purpose of the study, the study procedure, and associated risks and provided written informed consent before participation.

PET/CT Protocol

This study was performed under Investigational New Drug 78,283. ^{11}C-DPA-713 was synthesized according to the procedures of Thominiaux et al. (14). Radiochemical purity was greater than 95%. A Discovery Rx VCT scanner (GE Healthcare), equipped with high-performance lutetium yttrium oxyorthosilicate PET crystals and a 64-slice CT component, was used. Subjects were positioned supine and imaged at rest. Before PET, a helical transmission CT scan (120 kVp; 20–200 mA, automatically adjusted) was acquired at each bed position. The CT scan was used for attenuation correction of the PET data and to delineate organ boundaries. ^{11}C-DPA-713 (injected dose, 668 ± 21 MBq; specific activity, 668 ± 21 GBq/μmol; mass dose, 0.985 ± 0.13 μg) was delivered as a bolus via a catheterized vein over an approximately 30-s injection time. The catheter could not be accessed readily with the subject positioned in the field of view. Thus, after the

TABLE 1
Summary of Subjects and Injected Dose of ^{11}C-DPA-713

Subject no.	Age (y)	Mass (kg)	Height (m)	Body mass index (kg/m²)	Injected dose (MBq)
F1	37	69.0	1.65	25.3	681
F2	31	90.9	1.52	39.3	652
F3	43	74.5	1.52	32.3	642
M1	34	86.0	1.88	24.3	695
M2	32	85.2	1.78	26.9	655
M3	37	86.5	1.68	30.7	681
Mean ± SD	36 ± 4	82.0 ± 8.4	1.67 ± 0.14	29.8 ± 5.6	668 ± 21

CT scan, the patient bed was positioned to allow access to the catheter for radiotracer injection. The bed was then moved back (~30 s) so that the PET acquisition was initiated about 1 min after radiotracer delivery. PET was performed using a sequence of 7 passes. For each pass, 8 or 9 contiguous single-bed-position PET images were acquired in 3-dimensional mode, with an 11-slice (5-mm) overlap. The scan durations per bed position for the 7 passes were 15, 30, 45, 60, 120, 240, and 240 s. PET images were reconstructed as described previously (15) using a 3-dimensional ordered-subset expectation maximization algorithm with 2 iterations, 21 subsets, a 3.0-mm postreconstruction gaussian filter, 4.7 × 4.7 mm (in-plane), and 3.27-mm (transaxial) voxels. To obtain images in Bq/mL, the scanner was calibrated with a 20-cm diameter, 20-cm-long ^{18}F water phantom. The activity was measured using a dose calibrator that had been previously calibrated for ^{18}F using a National Institute of Standards and Technology–traceable source.

Regions of Interest (ROIs)

ROI analysis was performed using Analyze 10.0 (Mayo Clinic Foundation) (16). Tissue ROIs were drawn on the standard regions used by OLINDA 1.1 (Vanderbilt University) for dosimetry calculation (17). To measure total disintegrations in gallbladder and urinary bladder contents, large ROIs were drawn to encompass the entire volume. For other organs, the regions were delineated by subsampling the organ, with care taken to ensure that the ROI included perceived regions of high radioactivity. Testes on male subjects and uterus, breast tissue, and ovaries on female subjects were identified. However, for 1 female subject (F2), ovaries could not be identified. To ensure a conservatively high dose estimate, the small intestine and stomach were subsampled by drawing ROIs that encompassed the organ wall and contents in slices of highest activity in each organ. Because ^{11}C-DPA-713 does not accumulate in bone, it was assumed that all femoral radioactivity was located in red marrow. ROIs were not drawn on muscle, skin, or thymus. For the purpose of validating the use of subsampled ROIs, whole-organ ROIs were drawn for 2 subjects (F2 and M3). All ROIs were applied to the dynamic data to generate time–activity curves. Time–activity curves were generated without decay correction, and the acquisition time was taken to be the midpoint time of the bed acquisition that contained the region. There were 11 overlap slices for adjacent beds, in which case the acquisition time was taken to be the average of the mid-point times of the 2 beds. A complicating factor in determining the acquisition time precisely is that in some cases, particularly for whole-organ ROIs, regions extended across both single-bed and overlap

regions, in which case the within-region radioactivity corresponds to 2 or more different time points. In that case, if most (>90%) of the region was located in a specific bed or overlap region, the corresponding time was used to generate the time–activity curves. If the region was split more evenly, then an average time weighted by the number of voxels at each bed or overlap region was used. In all subjects, we noticed that the catheter tubing and the site of catheter insertion were clearly visible throughout the study. This visibility indicates that some residual activity remained in the catheter and thus did not effectively enter the circulatory system. To determine the catheter residual, an ROI was drawn around the tubing and injection site. The total radioactivity remaining in the catheter was then compared with the total injected radioactivity, accounting for radioactive decay. The mean percentage activity remaining in the catheter was 2.4% ± 2.3%, with individual values ranging from 0.5% to 6.2%. For the purpose of dose normalization required for computing residence times, the injected ^{11}C-DPA-713 radioactivity was adjusted by subtracting the measured catheter residual radioactivity. With subtraction of the catheter activity, the percentage injected dose to all organs is increased because the radiotracer uptake is attributed effectively to a smaller injected dose.

Residence Times and Absorbed Dose Calculations

To compute residence times, time–activity curves were expressed as percentage of the injected dose and then multiplied by the organ volume. We used sex-specific organ masses (adult women, adult men) that were provided in OLINDA and are based on a 56.9-kg woman and a 73.7-kg man. To convert standard organ mass to standard volume, each organ mass was divided by organ-specific tissue densities (18,19). After multiplying by the standard volumes, time–activity curves were integrated using trapezoidal integration up to the last measurement time point. Beyond the last time point, the integral to infinity was computed assuming exponential decay of ^{11}C with a half-life of 20.3 min. The total sum integral for each organ is the residence time. For gallbladder contents and urinary bladder contents, instead of normalizing to standard volumes, total disintegrations were estimated from the large ROIs that were drawn about those regions. For dosimetry calculation, we made the most conservative assumption that the entire dose was deposited in tissue, thus giving the maximum possible residence time of 0.488 h (i.e., half-life/ln(2)) (ln(2) = 0.693 is the natural log of 2). The remainder-of-body radioactivity was thus computed as the sum of the residence times in all identified tissues, subtracted from 0.488. For each subject, the residence times were
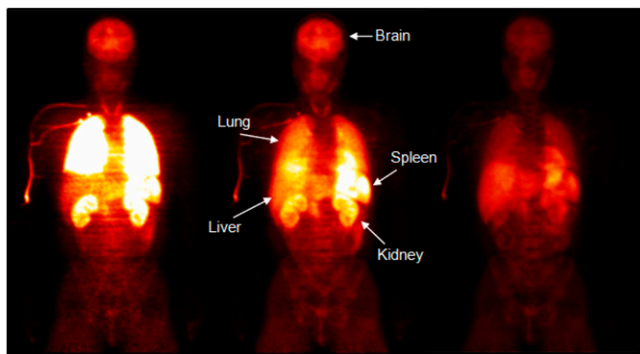
FIGURE 1. Summed coronal 2-dimensional projections of tracer activity after bolus injection of ^{11}C-DPA-713. Seven whole-body passes were performed as described. Images from left to right are from passes 1, 3, and 5 and show tracer biodistribution from 1 to 3, from 10 to 16, and from 28 to 42 min after injection, respectively. Images are displayed to same maximum. Lung uptake is prominent immediately after injection. Substantial tracer uptake is also observed in kidneys, spleen, liver, and brain.

input to OLINDA using a sex-specific model (adult women, adult men), and the effective dose equivalent was based on the tissue-weighting factors recommended in International Commission on Radiological Protection (ICRP) publication 60 (20). We report mean ± SD of residence times and effective dose equivalent values averaged across all subjects. For comparison of dose estimates obtained with whole-organ and subsampled ROIs, we take the values obtained with whole-organ ROIs as the standard values

and compute the percentage difference in the dose estimates obtained with subsampled ROIs.

RESULTS

The whole-body biodistribution of ^{11}C-DPA-713 is shown in 2-dimensional coronal projections in Figure 1. Tissue residence times are shown in Table 2, and the absorbed dose estimates are in Table 3. Figure 2 shows the whole-organ uptake curves expressed as a percentage of the injected dose; these are the curves that are integrated to compute residence times. The highest residence times were obtained in the lungs, liver, red marrow, brain, kidney, and small intestine. The highest absorbed doses were obtained in the lungs, spleen, kidney, pancreas, heart, and liver. For the 2 subjects (F2 and M3, Table 1) who had whole-organ ROIs drawn, the total-body dose estimates and the effective dose obtained using either whole-organ or subsampled ROIs agreed to within 1%. The effective dose equivalent obtained with either method agreed within 10% for both subjects (F2, 2.4%; M3, 9.0%), with subsampling giving the larger dose estimate. The individual organ dose estimates were also similar, with 75% of the organ doses agreeing to within 10% with either whole-organ or subsampled ROIs. Of particular importance to ^{11}C-DPA-713 dosimetry is that the lungs were again determined to be the critical dose-limiting organ, with dose estimates

TABLE 2
[11]C-DPA-713 Residence Times in Measured Tissues (Hours)

Tissue or region	Men (n = 3)	Women (n = 3)	Mean ± SD (n = 6)
Adrenals	3.55E–04	3.57E–04	3.56E–04 ± 1.50E–04
Brain	1.27E–02	1.09E–02	1.18E–02 ± 3.77E–03
Breasts	—	1.09E–03	1.09E–03 ± 7.15E–04
Gallbladder contents	1.73E–04	9.97E–05	1.36E–04 ± 1.24E–04
Lower large intestine wall	8.63E–04	1.58E–03	1.22E–03 ± 7.45E–04
Small intestine	8.64E–03	1.26E–02	1.06E–02 ± 3.72E–03
Stomach	3.92E–03	2.10E–03	3.01E–03 ± 1.25E–03
Upper large intestine wall	1.89E–03	4.13E–03	3.01E–03 ± 3.56E–03
Heart contents	3.71E–03	3.55E–03	3.63E–03 ± 2.17E–03
Heart wall	6.68E–03	6.10E–03	6.39E–03 ± 3.64E–03
Kidneys	1.15E–02	1.01E–02	1.08E–02 ± 3.11E–03
Liver	4.69E–02	3.50E–02	4.10E–02 ± 1.04E–02
Lungs	6.87E–02	6.36E–02	6.62E–02 ± 2.20E–02
Ovaries	—	8.90E–05	8.90E–05 ± 5.80E–05*
Pancreas	3.43E–03	2.72E–03	3.08E–03 ± 1.41E–03
Red marrow	1.14E–02	1.94E–02	1.54E–02 ± 9.16E–03
Spleen	7.99E–03	6.17E–03	7.08E–03 ± 2.19E–03
Testes	1.83E–04	—	1.83E–04 ± 2.52E–05
Thyroid	4.17E–04	3.40E–04	3.79E–04 ± 1.52E–04
Urinary bladder contents	2.19E–04	1.26E–04	1.72E–04 ± 1.21E–04
Uterus or uterine wall	—	7.33E–04	7.33E–04 ± 1.75E–04
Remainder of body	0.298	0.307	0.303 ± 0.050

*Ovaries were not identified positively in 1 female subject (F2); thus, mean ovarian residence time is based on measurements from 2 subjects. Mean values for sex-specific regions, including breasts, uterus or uterine wall, and testes, are based on measurements from 3 subjects of each sex.

TABLE 3
Absorbed Dose Estimates After Bolus Injection of ^{11}C-DPA-713

Organ	mSv/MBq	rem/mCi	Percentage of coefficient of variation
Adrenals	8.21E–03	3.04E–02	33.0
Brain	3.34E–03	1.24E–02	25.9
Breasts	2.07E–03	7.64E–03	21.1
Gallbladder wall	4.00E–03	1.48E–02	7.1
Lower large intestine wall	3.81E–03	1.41E–02	26.6
Small intestine	6.19E–03	2.29E–02	25.7
Stomach	4.72E–03	1.75E–02	9.1
Upper large intestine wall	4.92E–03	1.82E–02	50.7
Heart	9.32E–03	3.45E–02	42.3
Kidneys	1.17E–02	4.34E–02	24.7
Liver	9.19E–03	3.41E–02	18.3
Lungs	2.01E–02	7.43E–02	28.8
Muscle	2.53E–03	9.35E–03	15.3
Ovaries	3.88E–03	1.44E–02	28.3
Pancreas	1.12E–02	4.13E–02	36.2
Red marrow	3.86E–03	1.43E–02	23.7
Bone surface	4.71E–03	1.74E–02	23.6
Skin	1.96E–03	7.25E–03	16.7
Spleen	1.32E–02	4.87E–02	25.1
Testes	2.00E–03	7.39E–03	1.6
Thymus	2.99E–03	1.11E–02	13.8
Thyroid	6.04E–03	2.24E–02	29.0
Urinary bladder wall	2.37E–03	8.76E–03	12.2
Uterus	4.19E–03	1.55E–02	14.1
Total	3.23E–03	1.20E–02	12.4
Effective dose equivalent	7.67E–03	2.84E–02	19.9
Effective dose	5.93E–03	2.20E–02	17.0

Coefficient of variation is equal to SD divided by mean multiplied by 100. Values are averaged across all 6 subjects, except for breasts, uterus or uterine wall, testes, and ovaries, which are sex-specific and thus averaged across 3 subjects. Although ovaries were not identified in 1 female subject, OLINDA is still able to report absorbed dose estimate for that subject; estimate was included for computing average dose.

using whole or subsampled regions agreeing to within 3% for both subjects (F2, 1.4%; M3, 2.3%).

DISCUSSION

The biodistribution of ^{11}C-DPA-713 was found to be generally consistent with the known distribution of TSPO (21–23). The dosimetry is also similar to that of the TSPO ligand ^{11}C-PBR28 (24), which is expected because ^{11}C-DPA-713 and ^{11}C-PBR28 have similar pharmacokinetics (11,25). In particular, for both ^{11}C-DPA-713 and ^{11}C-PBR28, the highest residence times were in the lungs and liver, and the highest absorbed doses were in the lungs, kidney, and spleen. For ^{11}C-DPA-713, the lungs were determined to be the dose-limiting organ. On the basis of a single exposure limit of 5 rem (50 mSv), the single-administration dose limit is 2.49 GBq, or 67.3 mCi. A typical human PET study is performed with 555–740 MBq (15–20 mCi); thus, multiple tracer injections are possible, making test–retest and longitudinal studies quite feasible. The allowed dose limit is similar to that of other ^{11}C-labeled radiotracers, and the effective dose of ^{11}C-DPA-713 (5.9 μSv/MBq) is virtually at the median of ^{11}C dosimetry values reported previously (as shown in Table 3 of Virta et al. (26) and also in Table 3 of Hirvonen et al. (27)).

Regarding tissues that are more radiation-sensitive, according to the Food and Drug Administration title 21 Code of Federal Regulations (CFR), part 361, only 3 rem are allowed in a single-dose administration to the whole body, active blood-forming organs, lens of the eye, and gonads (28). When needed for dosimetry reports, it is recommended that the brain dose be used as an estimate of the lens-of-eye dose. Even if the more stringent public lens-of-eye exposure (15 mSv) recommended by ICRP publication 103 (29) is applied, the single-dose limit is 4.49 GBq (121 mCi); thus, the lens of the eye is not dose-limiting relative to the lungs. The organ-weighting factors recommended in ICRP 103 (29) were not applied here, but it was found for ^{11}C-R-PK11195 that the effective dose estimates obtained with either ICRP 60 or ICRP 103 weighting factors are nearly identical (27). ^{11}C-DPA-713 is also nontoxic, because the no-observed-effect-limit dose is 49.3 μg/kg/d according to the SRI international study (30). At typical specific activity levels, approximately 1 μg is injected in a human study.
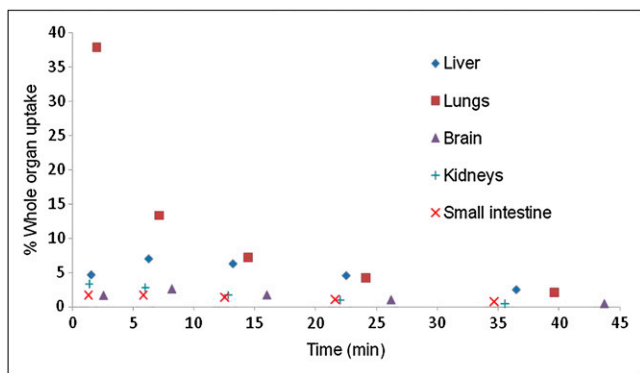
FIGURE 2. Whole-organ uptake after bolus injection of ^{11}C-DPA-713. Values are total organ activity expressed as percentage of initial bolus activity. For each subject, 7 whole-body dynamic scans were obtained, with 8–9 bed positions that proceeded from thigh to head. Thus, brain was imaged in last bed position. Plot shows first 5 whole-body passes, and values reflect average of all 6 subjects. Both axes are averaged, because the postinjection scan times are slightly different for each subject.

Drawing subsampled regions, as opposed to the time-consuming method of delineating whole-organ boundaries, is a practical approach to measuring activity in various organs (*31–33*). For the 2 subjects who were examined (F2 and M3) with whole-organ ROIs, the total-body dose and the effective dose were within 1% of the values obtained from subsampled ROIs. The lung dose was also quite similar, with subsampled ROIs yielding a 2% higher absorbed dose estimate. To further assess if subsampling was sufficient to quantify the dose to the critical organ, a whole-lung region was created for all subjects using the semiautomated ROI thresholding tool in Analyze (*16*). Lung residence times using the whole-lung ROIs were 6.1% less than the residence times obtained with subsampling; thus, the lung dose was not underestimated by subsampling.

To simplify the labor-intensive procedure of generating non–decay-corrected time–activity curves with acquisition times corresponding to specific bed positions, we attempted to perform the dosimetry with the time–activity curves decay-corrected to the start of each pass. In principle, that will yield the same residence time integral as non–decay-corrected data if there is negligible tracer redistribution from the start of the pass to the time of the specific bed acquisition. The benefit of decay correction to the start of each pass is that the activity throughout the body corresponds to the same time. That is, this procedure removes the ambiguity of the acquisition time when an organ is imaged in adjacent beds. In general, the dosimetry values were quite similar to those obtained without decay correction. However, for the lungs, performing the decay correction led to a consistent underestimation (>10%) in absorbed dose. Because the lungs are the critical organ, the result was a corresponding increase in the allowed dose limit. Thus, we used the non–decay-corrected results to ensure we obtained the most conservative, as well as the most accurate, dose estimate.

The biodistribution of ^{11}C-DPA-713 is similar to that of other TSPO ligands, as is evident when comparing whole-body images of the present study (Fig. 1) with the corresponding figures for [11]C-*R*-PK11195 (*27*) and ^{11}C-PBR28 (*24*). However, in contrast to the present study that found the lungs to be the critical organ, for both [11]C-*R*-PK11195 and ^{11}C-PBR28 the critical organ was the kidneys, with the spleen receiving the next highest dose. A comparison of whole-body biodistribution showed that [11]C-*R*-PK11195 has low lung uptake, compared with ^{11}C-PBR28 (*34*); thus, it is not surprising that the lungs are not the critical organ for [11]C-*R*-PK11195 dosimetry. On the other hand, ^{11}C-PBR28 and ^{11}C-DPA-713 share some similar properties, including similar affinity and lipophilicity (*11*). ^{11}C-PBR28 and ^{11}C-DPA-713 do, however, show differences in protein binding (*11*), pharmacokinetics of labeled metabolites (*25*), and sensitivity to multiaffinity state binding (*12*). Differences in methodology for dosimetry calculation may also contribute to the determination of different critical organs for ^{11}C-PBR28 and ^{11}C-DPA-713. For ^{11}C-PBR28, it has been reported that the binding affinity affects dosimetry calculation (*24*). In particular, in a single subject with low binding affinity binding, there was a large decrease in dose to the spleen, kidney, and lungs, with a corresponding increased dose to the liver, gallbladder wall, and urinary bladder wall. Furthermore, the effective dose was reported to be 28% less. PBR28 has a particularly large ratio in TSPO binding affinity (50-fold) between low- and high-affinity states (*12*). ^{11}C-DPA-713 has only a 4-fold ratio; thus, the impact of affinity on dosimetry estimates should be attenuated considerably. In the present study, on the basis of the consistency of tracer uptake in the brain and lungs, all subjects are believed to exhibit high-affinity binding. In principle, ^{11}C-DPA-713 and ^{11}C-PBR28 have favorable properties to be effective PET agents (*11*), although the presence of multiple-affinity-state binding has confounded efforts to demonstrate clearly that these tracers will improve on [11]C-*R*-PK11195 for clinical investigation. Another TSPO ligand that may affect the future use of ^{11}C-DPA-713 is the compound ^{18}F-DPA-714, which has a similar chemical structure (*35*). ^{18}F-DPA-714 has an inherent advantage for clinical use because of labeling with ^{18}F, whereas ^{11}C-DPA-713 is amenable to research protocols that call for multiple PET studies on the same day. Both ^{11}C-DPA-713 and ^{18}F-DPA-714 have been shown to give improved contrast over [11]C-*R*-PK11195 in animal models of neuroinflammation (*36,37*). DPA-714 increases pregnenolone synthesis, which is indicative of a TSPO agonist, whereas DPA-713 has no effect and appears to be an antagonist (*38*). In that case, ^{11}C-DPA-713 and ^{18}F-DPA-714 have the potential to provide complementary information.

CONCLUSION

Absorbed dose estimates after ^{11}C-DPA-713 bolus injection reveal the lungs to be the critical organ, yielding a single-

injected-dose limit of 2,487.6 MBq (67.3 mCi). The dosimetry is consistent with other ^{11}C tracers and indicates that multiple injections per year are easily allowable under current federal guidelines (21CFR361.1), especially given that typical radiotracer injections are no more than 740 MBq (20 mCi).

DISCLOSURE STATEMENT

ACKNOWLEDGMENTS

REFERENCES

1. Papadopoulos V, Baraldi M, Guilarte TR, et al. Translocator protein (18kDa): new nomenclature for the peripheral-type benzodiazepine receptor based on its structure and molecular function. *Trends Pharmacol Sci.* 2006;27:402–409.
2. Banati RB. Visualising microglial activation in vivo. *Glia.* 2002;40:206–217.
3. Cagnin A, Gerhard A, Banati RB. In vivo imaging of neuroinflammation. *Eur Neuropsychopharmacol.* 2002;12:581–586.
4. Scarf AM, Kassiou M. The translocator protein. *J Nucl Med.* 2011;52:677–680.
5. Weissman BA, Raveh L. Peripheral benzodiazepine receptors: on mice and human brain imaging. *J Neurochem.* 2003;84:432–437.
6. Chauveau F, Boutin H, Van Camp N, Dolle F, Tavitian B. Nuclear imaging of neuroinflammation: a comprehensive review of [^{11}C]PK11195 challengers. *Eur J Nucl Med Mol Imaging.* 2008;35:2304–2319.
7. Dollé F, Luus C, Reynolds A, Kassiou M. Radiolabelled molecules for imaging the translocator protein (18 kDa) using positron emission tomography. *Curr Med Chem.* 2009;16:2899–2923.
8. Doorduin J, de Vries EF, Dierckx RA, Klein HC. PET imaging of the peripheral benzodiazepine receptor: monitoring disease progression and therapy response in neurodegenerative disorders. *Curr Pharm Des.* 2008;14:3297–3315.
9. Luus C, Hanani R, Reynolds A, Kassiou M. The development of PET radioligands for imaging the translocator protein (18 kDa): what have we learned? *J Labelled Comp Rad.* 2010;53:501–510.
10. James ML, Fulton RR, Henderson DJ, et al. Synthesis and in vivo evaluation of a novel peripheral benzodiazepine receptor PET radioligand. *Bioorg Med Chem.* 2005;13:6188–6194.
11. Endres CJ, Pomper MG, James M, et al. Initial evaluation of ^{11}C-DPA-713, a novel TSPO PET ligand, in humans. *J Nucl Med.* 2009;50:1276–1282.
12. Owen DR, Gunn RN, Rabiner EA, et al. Mixed-affinity binding in humans with 18-kDa translocator protein ligands. *J Nucl Med.* 2011;52:24–32.
13. Owen DR, Howell OW, Tang SP, et al. Two binding sites for [^{3}H]PBR28 in human brain: implications for TSPO PET imaging of neuroinflammation. *J Cereb Blood Flow Metab.* 2010;30:1608–1618.
14. Thominiaux C, Dolle F, James ML, et al. Improved synthesis of the peripheral benzodiazepine receptor ligand [^{11}C]DPA-713 using [^{11}C]methyl triflate. *Appl Radiat Isot.* 2006;64:570–573.
15. Lodge MA, Chaudhry MA, Udall DN, Wahl RL. Characterization of a perirectal artifact in ^{18}F-FDG PET/CT. *J Nucl Med.* 2010;51:1501–1506.
16. Robb RA, Hanson DP, Karwoski RA, Larson AG, Workman EL, Stacy MC. Analyze: a comprehensive, operator-interactive software package for multidimensional medical image display and analysis. *Comput Med Imaging Graph.* 1989;13:433–454.
17. Stabin MG, Sparks RB, Crowe E. OLINDA/EXM: the second-generation personal computer software for internal dose assessment in nuclear medicine. *J Nucl Med.* 2005;46:1023–1027.
18. International Commission on Radiological Protection (ICRP). Basic anatomical and physiological data for use in radiological protection reference values. ICRP publication 89. *Ann ICRP.* 2002;32:3–4.
19. Marine PM, Stabin MG, Fernald MJ, Brill AB. Changes in radiation dose with variations in human anatomy: larger and smaller normal-stature adults. *J Nucl Med.* 2010;51:806–811.
20. International Commission on Radiological Protection (ICRP). 1990 Recommendations of the International Commission on Radiological Protection. ICRP publication 60. *Ann ICRP.* 1991;21:1–3.
21. Anholt RR, De Souza EB, Oster-Granite ML, Snyder SH. Peripheral-type benzodiazepine receptors: autoradiographic localization in whole-body sections of neonatal rats. *J Pharmacol Exp Ther.* 1985;233:517–526.
22. Bribes E, Carriere D, Goubet C, Galiegue S, Casellas P, Simony-Lafontaine J. Immunohistochemical assessment of the peripheral benzodiazepine receptor in human tissues. *J Histochem Cytochem.* 2004;52:19–28.
23. Liu J, Matyakhina L, Han Z, et al. Molecular cloning, chromosomal localization of human peripheral-type benzodiazepine receptor and PKA regulatory subunit type 1A (PRKAR1A)-associated protein PAP7, and studies in PRKAR1A mutant cells and tissues. *FASEB J.* 2003;17:1189–1191.
24. Brown AK, Fujita M, Fujimura Y, et al. Radiation dosimetry and biodistribution in monkey and man of ^{11}C-PBR28: a PET radioligand to image inflammation. *J Nucl Med.* 2007;48:2072–2079.
25. Fujita M, Imaizumi M, Zoghbi SS, et al. Kinetic analysis in healthy humans of a novel positron emission tomography radioligand to image the peripheral benzodiazepine receptor, a potential biomarker for inflammation. *Neuroimage.* 2008;40:43–52.
26. Virta JR, Tolvanen T, Nagren K, Bruck A, Roivainen A, Rinne JO. 1-^{11}C-methyl-4-piperidinyl-N-butyrate radiation dosimetry in humans by dynamic organ-specific evaluation. *J Nucl Med.* 2008;49:347–353.
27. Hirvonen J, Roivainen A, Virta J, Helin S, Nagren K, Rinne JO. Human biodistribution and radiation dosimetry of [11]C-(R)-PK11195, the prototypic PET ligand to image inflammation. *Eur J Nucl Med Mol Imaging.* 2010;37:606–612.
28. Food and Drug Administration. *Radioactive Drugs for Certain Research Uses. Title 21 CFR 361.1.* Washington, DC: National Archives and Records Administration; 2001.
29. International Commission on Radiological Protection (ICRP). The 2007 Recommendations of the International Commission on Radiological Protection. ICRP publication 103. *Ann ICRP.* 2007;37:2–4.
30. Ng HH. *Intravenous Toxicity Study of DPA-713 in Sprague-Dawley Rats.* Menlo Park, CA: SRI International; 2006. SRI study number M420-05.
31. Laymon CM, Mason NS, Frankle WG, et al. Human biodistribution and dosimetry of the D2/3 agonist ^{11}C-N-propylnorapomorphine (^{11}C-NPA) determined from PET. *J Nucl Med.* 2009;50:814–817.
32. Laymon CM, Narendran R, Mason NS, et al. Human biodistribution and dosimetry of the PET radioligand [^{11}C]flumazenil (FMZ). *Mol Imaging Biol.* March 2, 2011 [Epub ahead of print].
33. Slifstein M, Hwang DR, Martinez D, et al. Biodistribution and radiation dosimetry of the dopamine D2 ligand ^{11}C-raclopride determined from human whole-body PET. *J Nucl Med.* 2006;47:313–319.
34. Kreisl WC, Fujita M, Fujimura Y, et al. Comparison of [^{11}C]-(R)-PK 11195 and [^{11}C]PBR28, two radioligands for translocator protein (18 kDa) in human and monkey: Implications for positron emission tomographic imaging of this inflammation biomarker. *Neuroimage.* 2010;49:2924–2932.
35. James ML, Fulton RR, Vercoullie J, et al. DPA-714, a new translocator protein-specific ligand: synthesis, radiofluorination, and pharmacologic characterization. *J Nucl Med.* 2008;49:814–822.
36. Chauveau F, Van Camp N, Dolle F, et al. Comparative evaluation of the translocator protein radioligands ^{11}C-DPA-713, ^{18}F-DPA-714, and ^{11}C-PK11195 in a rat model of acute neuroinflammation. *J Nucl Med.* 2009;50:468–476.
37. Doorduin J, Klein HC, Dierckx RA, James M, Kassiou M, de Vries EF. [^{11}C]-DPA-713 and [^{18}F]-DPA-714 as new PET tracers for TSPO: a comparison with [^{11}C]-(R)-PK11195 in a rat model of herpes encephalitis. *Mol Imaging Biol.* 2009;11:386–398.
38. Reynolds A, Hanani R, Hibbs D, et al. Pyrazolo[1,5-a]pyrimidine acetamides: 4-Phenyl alkyl ether derivatives as potent ligands for the 18 kDa translocator protein (TSPO). *Bioorg Med Chem Lett.* 2010;20:5799–5802.